RESEARCH PAPER

Capillary focusing close to a topographic step: shape and instability of confined liquid filaments

Michael Hein · Shahriar Afkhami · Ralf Seemann · Lou Kondic

Abstract Step-emulsification is a microfluidic technique for droplet generation which relies on the abrupt decrease of confinement of a liquid filament surrounded by a continuous phase. A striking feature of this geometry is the transition between two distinct droplet breakup regimes, the "step-regime" and "jet-regime," at a critical capillary number. In the step-regime, small and monodisperse droplets break off from the filament directly at a topographic step, while in the jet-regime a jet protrudes into the larger channel region and large plug-like droplets are produced. We characterize the breakup behavior as a function of the filament geometry and the capillary number and present experimental results on the shape and evolution of the filament for a wide range of capillary numbers in the jet-regime. We compare the experimental results with numerical simulations. Assumptions based on the smallness of the depth of the microfluidic channel allow us to reduce the governing equations to the Hele-Shaw problem with surface tension. The full nonlinear equations are then solved numerically using a volume-of-fluid-based algorithm. The computational framework also captures the transition between both regimes, offering a deeper understanding of the underlying breakup mechanism.
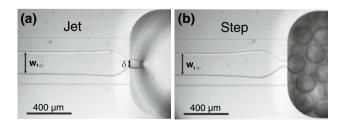
1 Introduction

Hydrodynamic instabilities leading to droplet formation by a decay of a liquid jet or filament have received considerable interest over the last two centuries (Rayleigh [1878]) and renewed especially since the emergence of two-phase microfluidic systems. Hydrodynamic instabilities are employed to generate droplets on the micro-scale, a technique that is promising for many lab-on-a-chip applications, where droplets could serve as discrete vials for chemical reactions or bio-analysis. Extensive reviews on experimental and theoretical studies of droplet production units and droplet handling in microfluidics have been written by Seemann et al. ([2012]) and Wörner ([2012]). Typically, three different droplet production units are being used: In a T-junction (Thorsen et al. [2001]), in which the dispersed phase enters a channel filled with a continuous phase from a side channel, droplets are typically produced either by shearing or by a "Plug-and-Squeeze mechanism" (Garstecki et al. [2006]). In co-flow or cross-flow geometries, which have received considerable interest from an experimental as well as from analytical perspective (Anna et al. [2003]; Guillot et al. [2007],

M. Hein · R. Seemann
Experimental Physics, Saarland University,
66123 Saarbrücken, Germany
e-mail: michael.hein@physik.uni-saarland.de

R. Seemann
e-mail: r.seemann@physik.uni-saarland.de

S. Afkhami (✉) · L. Kondic
Department of Mathematical Sciences, New Jersey Institute of Technology, Newark, NJ 07102, USA
e-mail: shahriar.afkhami@njit.edu

L. Kondic
e-mail: kondic@njit.edu

R. Seemann
Max Planck Institute for Dynamics and Self-Organization,
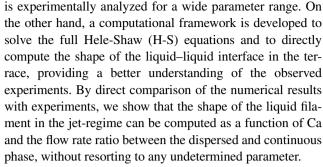37077 Göttingen, Germany

Springer

2008), the dispersed phase flows parallel to the continuous phase and decays into droplets either directly at the inlet ("Dripping"), forms a jet that decays some distance downstream ("Jetting") or forms a liquid jet, which is absolutely stable ("Co-Flow"). All of these methods are widely used.

The instability of a liquid filament confined in a quasi-two-dimensional geometry triggered by a sudden expansion of the channel has recently been described (Priest et al. 2006; Malloggi et al. 2010; Humphry et al. 2009; Shui et al. 2011; Dangla et al. 2013). The system consists of a shallow terrace and a larger microfluidic reservoir downstream, as shown in Fig. 1. In the terrace, the non-wetting dispersed liquid flows as a straight filament confined at the top and the bottom by the walls and surrounded by a continuous phase. The main control parameter is the capillary number, Ca, which represents the effect of viscous relative to capillary forces. Two distinct droplet breakup mechanisms can be observed for droplet generation. At high Ca, a mechanism called "jet-emulsification" occurs, in which the dispersed phase creates a stable tongue in the terrace. This tongue narrows to a neck close to the topographic step due to capillary focusing. From this neck, a jet protrudes, generating large and polydisperse droplets that fill the whole reservoir channel (see Fig. 1a). Below a critical Ca, the so-called "step-emulsification" occurs (see Fig. 1b). In the latter case, the inner stream forms a droplet immediately after it reaches the topographic step, where the tip then becomes unstable, producing droplets at high throughput with a monodispersity superior to the previously mentioned droplet production methods (Priest et al. 2006; Dangla et al. 2013). Recent efforts to describe this emulsification process have resulted in models for predicting lower bounds for the generated droplet size in the step-regime (Dangla et al. 2013) and estimating the width of the tongue at the step in the jet-regime (Malloggi et al. 2010). However, rigorous study of the shape and instability of the confined tongue and comprehensive comparison of experimental results with theoretical models have not been carried out until now.

In this article, we study the capillary focusing phenomena in a step-emulsification microfluidic device. On one hand, the dynamic filament shape and stability in the jet-regime

is experimentally analyzed for a wide parameter range. On the other hand, a computational framework is developed to solve the full Hele-Shaw (H-S) equations and to directly compute the shape of the liquid–liquid interface in the terrace, providing a better understanding of the observed experiments. By direct comparison of the numerical results with experiments, we show that the shape of the liquid filament in the jet-regime can be computed as a function of Ca and the flow rate ratio between the dispersed and continuous phase, without resorting to any undetermined parameter.

Here, a simple stability criterion is used to show that the experimentally observed transition between the step- and jet-regime can also be predicted by the numerical simulations; the description of this transition based on the direct numerical solution of the two-phase H-S equations with surface tension has not been addressed before.

2 Experimental method

To characterize the droplet breakup regimes in a step-emulsification geometry and the filament shape in the jet-regime, experiments are performed using a device micromachined into a polymethylmethacrylate (PMMA)-block with a terrace of width $w = 400\,\mu m$ and depth $b = 30\,\mu m$ (i.e., with aspect ratio $w/b = 12.76$) and a downstream reservoir of cross-sectional area of about $(1 \times 1)\,mm^2$. The channel is sealed by a PMMA-sheet. An aqueous phase with 28 wt% glycerol is injected as a dispersed phase into an oily continuous phase, IsoparM (ExxonMobil Chemical). For the chosen liquid system, the viscosity of the dispersed phase, μ_1, is matched with the viscosity of the continuous phase, μ_2, and is approximately 2.1 mPas. 2 wt% of the surfactant Span 80 (Sigma Aldrich) are added to the continuous phase to increase the droplet stability and to ensure the wetting of the channel walls by the continuous phase. The interfacial tension coefficient, γ, determined using the pendant drop method, is (3.5 ± 0.1) mN/m. The evolution of the interface is imaged using a microscope (Zeiss Axiovert) and a high-speed CMOS camera (PCO 1,200hs). The interface profiles as well as the tongue width, $w_{1\infty}$, far away from the neck, and the neck width, δ, directly at the step, are automatically measured using numerical image analysis (see Fig. 1a). Volumetric flow rates, Q_1 and Q_2, of the dispersed and the continuous phase, respectively, are adjusted using computer controlled syringe pumps. The corresponding Ca $= U_1\mu_1/\gamma$ is determined from the average flow velocity of the dispersed phase, U_1.

Fig. 1 Optical micrographs showing two regimes of droplet production. **a** "Jet-emulsification" for large Ca: breakup occurs downstream, **b** "Step-emulsification" for low Ca: breakup occurs at the step

3 Computational framework

In addition to physical experiments, a computational framework is developed to provide a deeper insight into the effects

governing the evolution of the liquid–liquid interface in the jet-regime and to predict the transition between the jet- and step-regime. The original governing equations are reduced to the time-dependent two-phase Hele-Shaw equations with the surface tension. We stress that, even in this case, the full problem is nonlinear due to the curvature term in the surface tension, and therefore, the full problem has to be solved numerically. Furthermore, although not considered here, our numerical model allows seamlessly varying the viscosity of both phases as well as the initial condition and the geometry of the Hele-Shaw problem. We use a volume-of-fluid (VOF)-based method to directly solve the governing equations. Our numerical model, described in detail by Afkhami and Renardy (2013), has the distinctive feature of being capable of, accurately and robustly, modeling the surface tension force. In addition, the accurate interface reconstruction, the second-order curvature computation, and the use of adaptive mesh refinement allow for resolved description of the interface, enabling us to investigate the complex features of interface profiles extracted from experiments, which was not possible in prior studies. The order of accuracy and convergence properties of the numerical methods were previously studied by Afkhami and Renardy (2013).

The computational framework consists of the classical H-S model to simulate the shape of the interface between the dispersed and the continuous phase in the shallow channel. The depth-averaged velocity field in both phases is defined as

$$\mathbf{u}(x,y,t) = \frac{b^2}{12\mu}\{-\nabla p(x,y,t) + \mathbf{F}(x,y,t)\}, \tag{1}$$

where μ is the viscosity of the considered phase defined as

$$\mu(f) = \frac{\mu_1\mu_2}{(1-f)\mu_1 + f\mu_2}, \tag{2}$$

where μ_1 and μ_2 refer to the viscosity of fluid 1 and 2, respectively, b is the depth of the H-S cell, and $p(x,y,t)$ is the local pressure. The VOF function, $f(x,y,t)$, tracks the motion of the interface. In a VOF method, the discrete form of the function f represents the volume fraction of a cell filled with, in this case, fluid 1. Away from the interface, $f = 0$ (inside fluid 2) or $f = 1$ (inside fluid 1); "interface cells" correspond to $0 < f < 1$. The evolution of f satisfies the advection equation

$$\frac{\partial f}{\partial t} + \mathbf{u}(x,y,t) \cdot \nabla f = 0. \tag{3}$$

In this formulation, surface tension enters as a singular body force, $\mathbf{F}(x,y,t)$, centered at the interface between two fluids (Afkhami and Renardy 2013). Figure 2 is a schematic of the flow domain, $0 \leq x \leq L, |y| \leq w/2$, representing the terrace. Due to symmetry, only half of the domain is simulated. We consider a constant pressure, p_0, in the
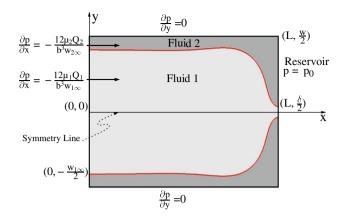

Fig. 2 Schematic of the flow domain for the Hele-Shaw model and the corresponding boundary conditions. The domain is bounded by walls at $|y| = w/2$. At $x = 0$, fluid 1 occupies $|y| \leq w_{1\infty}/2$ and fluid 2 occupies $w_{1\infty}/2 < y \leq w$ and $-w < y < -w_{1\infty}/2$; $w_{2\infty} = w - w_{1\infty}$

reservoir and, as a first approximation for the outflow into a reservoir, an outflow pressure boundary condition at the exit, $x = L$, as

$$p(x,y,t) = \begin{cases} p_0 + 2A\gamma/b & 0 < f \leq 1 \\ p_0 & f = 0 \end{cases} \tag{4}$$

where the out-of-plane curvature is given by $2/b$. Thus $2\gamma/b$ is the Laplace pressure inside the dispersed phase 1. Since the in-plane curvature at the step is typically much smaller than the out-of-plane curvature, it can be safely neglected. A pressure correction parameter, $A \leq 1$, is included for modeling the flow configurations for which the H-S approximation is expected to be less accurate, as discussed further below. The boundary condition for f at the top and bottom walls is $f = 0$. At the outflow, the boundary condition for f is the interface being perpendicular to the topographic step: $\partial f/\partial x = 0$. This is justified experimentally in Sect. 4.1. On the solid boundaries (side walls), $\partial p/\partial y = 0$. At the inlet, $x = 0$, the parallel flow solution holds, meaning that for both phases, the pressure gradient is prescribed as $\partial p(x,y,t)_i/\partial x = -(12\mu Q_i)/(b^3 w_{i\infty})$ where $i = (1,2), w_{i\infty}$ is the width occupied by the ith liquid at the inlet and Q_i is the flow rate of the ith phase. As in the experiments, we chose $dp_1/dx|_{x=0} = dp_2/dx|_{x=0}$ and fix b and w. The initial condition at $t = 0$ is a flat interface defined by the initial distribution of f over the domain. We keep L large enough so the results are unaffected by its value.

4 Results and discussion

4.1 Filament shape: temporal evolution

In the jet-regime, i.e., at sufficiently high Ca (see Fig. 1a), a filament of a dispersed phase, sandwiched by the
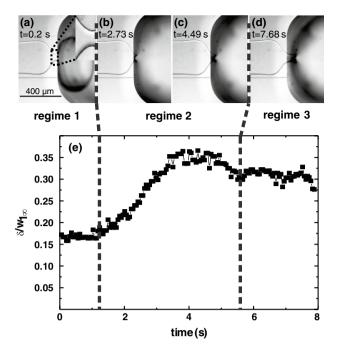
Fig. 3 Temporal evolution of the tongue in the jet-regime. **a–d** Micrographs with the *inset* showing the interface directly at the step and **e** the shape factor, $\delta/w_{1\infty}$, as a function of time; $Ca = 9.73 \times 10^{-3}$ and $Q_{1\infty}/Q_{2\infty} = 3$

continuous phase, is stable over the terrace due to the geometric confinement of the flow. When pushed into the reservoir, in which the pressure is presumably constant, the two phases are forced to balance their pressure. The dispersed phase, however, experiences a higher pressure due to the Laplace pressure, generated by the out-of-plane curvature of the interface and the evolving meniscus. This induces a temporarily varying cross-stream pressure difference between the two fluids. Thus, to adjust to a constant pressure at the step, the dispersed phase has to increase its velocity, whereas the continuous phase moves more slowly over the terrace. Due to mass conservation, the interface between the two fluids must assume a tongue-like shape that narrows down to a thin neck along the mean flow, an effect known as "capillary focusing."
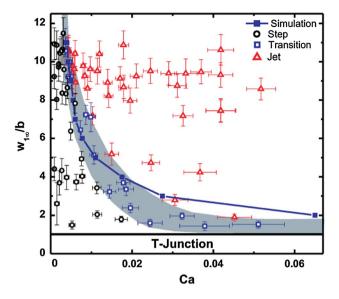
For droplet formation in an actual microfluidic device, the situation is more complex, since droplets are periodically formed in the reservoir, thus influencing the pressure at the step and consequently the tongue shape. Figure 3a–d shows a typical evolution of the tongue shape during droplet production in the jet-regime (see also the movie in the supplemental material). Figure 3e shows the tongue width (normalized by the filament width), $\delta/w_{1\infty}$, called the tongue shape factor, as a function of time. As shown, at the beginning of the droplet formation cycle (see Fig. 3a and regime 1 in Fig. 3e), when the droplet is initially pushed into the reservoir, $\delta/w_{1\infty}$ remains constant

while the droplet inflates, maintaining a nearly spherical shape. During this inflation process, the liquid–liquid interface at the step is perpendicular to the topographic step (see the inset in Fig. 3a). The Laplace pressure that counteracts the inflation of the droplet rapidly decreases as the droplet radius increases and remains merely constant when the droplet reaches the reservoir dimension. Additional complexity may arise in the case of droplet collision in the reservoir channel. When the droplet touches the walls of the reservoir, $\delta/w_{1\infty}$ typically increases as the droplet starts to travel downstream, pulling the tongue toward the step (see Fig. 3b, c and regime 2 in Fig. 3e). Additionally, the droplet blocks the reservoir, except for small regions along the corners of the rectangular reservoir. Thus, an additional pressure contribution, that is expected to increase with the droplet length (Labrot et al. 2009), is needed to push the continuous phase at constant flow rate downstream in the reservoir. This pressure component is also expected to deform the interface in the shallow terrace. Thus $\delta/w_{1\infty}$ reaches a maximum during regime 2 in Fig. 3e and then decreases, showing the formation of a neck, that may evolve to a stable width in regime 3 in Fig. 3e. In regime 3, the neck elongates as the rear interface of the droplet travels downstream, until it bulges and finally ruptures (see Fig. 3d and regime 3 in Fig. 3e). After droplet breakup, the process repeats starting in regime 1. From the above description of the tongue evolution in the jet-regime at high Ca, it is obvious that only in regime 1 the pressure boundary condition at the topographic step is known a priori, resembling an open outlet with a constant pressure, p_0. Thus, the experimental data taken in regime 1 are used for further comparison with computational results. In regimes 2 and 3, however, the pressure at the topographic step is significantly influenced by the evolving droplet in the reservoir. We note that regime 1 can be further expanded by increasing reservoir dimensions.

4.2 Transition from jet- to step-regime

A sudden transition to the step-regime occurs when reducing the Ca below a certain threshold, as shown in Fig. 4. The transition between jet- and step-regime can be qualitatively described as follows: At low Ca, when the width of the neck, δ, becomes comparable to the height of the terrace, b, the dispersed phase forms a nearly cylindrical neck, which is prone to a surface-tension-driven instability. As the neck is no longer stable, the filament breaks up rapidly and small droplets are continuously produced, accompanied by a periodic retraction of the tongue. We have confirmed this critical neck width experimentally by measuring δ in the metastable transition regime, where step- and jet-regime alternate (see shaded region in Fig. 4). Interestingly, despite the qualitative differences in tongue shape
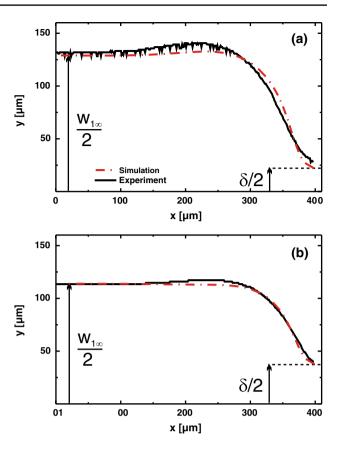
Fig. 4 Phase diagram demonstrating the transition of jet-regime (*red triangles*) to step-regime (*black circles*). *Blue open squares* denote the transition regime, where droplet production alternates between step- and jet-regime. *Blue solid squares* indicate the simulation results for $A = 0.4$, as discussed in the text. For $w_{1\infty}/b \leq 1$, no stable filament is formed (color figure online)

and stability between step- and jet-regime (cf. Fig. 1), we note that the tongue width far upstream from the step, $w_{1\infty}$, stays constant for a given $Q_{1\infty}/Q_{2\infty}$ when varying Ca. In particular, $w_{1\infty}$ is unaffected by the transition from the jet- to step-regime, which allows characterizing the transition as a function of the rescaled tongue width, $w_{1\infty}/b$, and Ca. Figure 4 shows the emulsification phase diagram in ($w_{1\infty}/b$, Ca) space, with an increased data range compared with Priest et al. (2006), in which it is shown that the phase diagram is insensitive to the viscosity ratio of the dispersed phase to the continuous phase, μ_1/μ_2. We note that for $w_{1\infty}/b \leq 1$, droplet breakup occurs at the inlet of the dispersed phase. This regime is comparable to breakup in a T-junction and is not considered here.

4.3 Comparison of experiments with numerical simulations

Figure 5 shows the direct comparison of the tongue profiles obtained from experiments with the corresponding simulations. As shown, the numerical simulations accurately reproduce the main features of the tongue shape, particularly the slight increase of the tongue width followed by the strong capillary focusing close to the topographic step. We also note that the agreement between the simulated results and experiments is best at higher Ca values, shown in Fig. 5b, remote from the transition to the step-regime, where the tongue width is larger and the validity of the H-S approximation (assumed in

Fig. 5 Comparison of the tongue profiles in the terrace obtained from experiments (*black solid line*) and simulations with $A = 1$ (*red dashed line*). Both experimental profiles are obtained in the jet-regime. **a** Ca $= 0.019$ and $w_{1\infty}/b = 7.97$ and **b** Ca $= 0.042$ and $w_{1\infty}/b = 7.44$. For experiments, $Q_{1\infty}/Q_{2\infty} = 1.5$. For simulations, $Q_{1\infty}/Q_{2\infty} = 1.67$ in (**a**) and $Q_{1\infty}/Q_{2\infty} = 1.41$ in (**b**) (color figure online)

the numerical scheme) is clearly fulfilled. To quantify the comparison between the numerical and experimental results, in Fig. 6, the shape factor, $\delta/w_{1\infty}$, measured from the obtained profiles, is plotted as a function of Ca. The error bars for the experimentally determined $\delta/w_{1\infty}$ are worst case estimates based on the width of the interface after image segmentation, and the error bars for Ca are Gaussian error estimates. The measured values for $\delta/w_{1\infty}$ agree within experimental accuracy with the results from the corresponding simulations, especially for medium to high Ca. Both the results from the experiment and the simulation show that the neck thickness increases with Ca, as also predicted analytically by Malloggi et al. (2010). However, for Ca $\lesssim 0.02$, close to the transition, simulation predicts a stronger focusing, i.e., a stronger decrease of $\delta/w_{1\infty}$ with Ca, when compared to the experimental data, as the neck becomes more and more cylindrical in this regime, making the H-S approximation less accurate. Thus, the numerical model underestimates
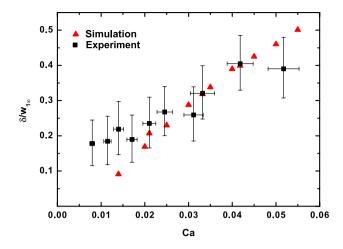
Fig. 6 Comparison of the experimentally determined shape factor, $\delta/w_{1\infty}$, for $Q_{1\infty}/Q_{2\infty} = 3$ (*black squares*) and the simulation results (*red triangles*) for $Q_{1\infty}/Q_{2\infty} = 2.81$ and $A = 1$ (color figure online)

$\delta/w_{1\infty}$ for small Ca. This underestimation can be compensated by introducing a pressure correction, A, as described in Eq. 4, which increases δ by weakening the capillary focusing, at the cost of a reduced bulging prior to the hydrodynamic focusing. We apply this pressure correction and use the stability criterion, $\delta = b$, as described in Sect. 4.2, and employ the numerical simulation to predict the transition from jet- to step-regime. Figure 4 shows the excellent agreement of the computationally predicted transition threshold when compared with experimental data for $A = 0.4$. As discussed previously, introducing A is needed when considering the regime where the H-S approximation is not strictly valid. A clear approach to improving the accuracy is to consider fully three-dimensional flow, as well as to consider possible influence of the viscosity contrast and capillary effects on the pressure correction factor. We leave these non-trivial extensions for future work.

5 Conclusion

In this article, the capillary focusing of a confined liquid filament at a topographic step is studied both experimentally and numerically. A novel computational framework, based on the Hele-Shaw approximation and the volume-of-fluid approach, is shown to predict experimental results quantitatively. We find that by modeling the reservoir with an applied pressure boundary condition, the computed shapes of the filament are in excellent agreement with experiments for moderate to high capillary numbers, without resorting to any undetermined parameters. Furthermore, we show that the numerical model can accurately predict the width of the tongue remote from the step. We

also characterize the width of the tongue at the step as a function of Ca and show that the computational results are in very good agreement with the experimental findings in the jet-regime and close to the transition to the step-regime. Direct computations also provide an accurate estimate of the transition between two distinct droplet breakup mechanisms characterized experimentally. This work is expected to set ground for further numerical and analytical treatment of confined filament shapes in similar geometries. The presented computational framework solves the full Hele-Shaw equations without additional simplifications. Thus, the model is not limited to predicting two-phase flow behavior in the specific geometry discussed in this paper and can easily be adapted to similar problems. Additionally, knowing the dependence of the breakup behaviour on filament geometry and capillary number will also facilitate application-specific designs of microfluidic droplet production units.

References

Afkhami S, Renardy Y (2013) A volume-of-fluid formulation for the study of co-flowing fluids governed by the Hele-Shaw equations. Phys Fluids 25:082001

Anna S, Bontoux N, Stone H (2003) Formation of dispersions using "flow focusing" in microchannels. Appl Phys Lett 82:364–366

Dangla R, Fradet E, Lopez Y, Baroud CN (2013) The physical mechanisms of step emulsification. J Phys D 46:114003

Garstecki P, Fuerstman MJ, Stone HA, Whitesides GM (2006) Formation of droplets and bubbles in a microfluidic T-junction-scaling and mechanism of break-up. Lab Chip 6:437–446

Guillot P, Colin A, Utada AS, Ajdari A (2007) Stability of a jet in confined pressure-driven biphasic flows at low Reynolds numbers. Phys Rev Lett 99:104502

Guillot P, Colin A, Ajdari A (2008) Stability of a jet in confined pressure-driven biphasic flows at low Reynolds number in various geometries. Phys Rev E 78:016307

Humphry KJ, Ajdari A, Fernández-Nieves A, Stone HA, Weitz DA (2009) Suppression of instabilities in multiphase flow by geometric confinement. Phys Rev E 79:056310

Labrot V, Schindler M, Guillot P, Colin A, Joanicot M (2009) Extracting the hydrodynamic resistance of droplets from their behavior in microchannel networks. Biomicrofluidics 3:012804

Malloggi F, Pannacci N, Attia R, Monti F, Mary P, Willaime H, Tabeling P (2010) Monodisperse colloids synthesized with nanofluidic technology. Langmuir 26:2369–2373

Priest C, Herminghaus S, Seemann R (2006) Generation of monodisperse gel emulsions in a microfluidic device. Appl Phys Lett 88:024106

Rayleigh L (1878) On the instability of jets. Proc Lond Math Soc 10:4–13

Seemann R, Brinkmann M, Pfohl T, Herminghaus S (2012) Droplet based microfluidics. Rep Prog Phys 75:016601

Shui L, van den Berg A, Eijkel JCT (2011) Scalable attoliter monodisperse droplet formation using multiphase nano-microfluidics. Microfluid Nanofluid 11:87–92

Thorsen T, Roberts RW, Arnold FH, Quake SR (2001) Dynamic pattern formation in a vesicle-generating microfluidic device. Phys Rev Lett 86:4163–4166

Wörner M (2012) Numerical modeling of multiphase flows in microfluidics and micro process engineering: a review of methods and applications. Microfluid Nanofluid 12:841–886